

Accepted Manuscript

An improved finite element space for discontinuous pressures

Roberto F. Ausas, Fabricio S. Sousa, Gustavo C. Buscaglia

PII: S0045-7825(09)00386-7

DOI: [10.1016/j.cma.2009.11.011](https://doi.org/10.1016/j.cma.2009.11.011)

Reference: CMA 9096

To appear in: *Comput. Methods Appl. Mech. Engrg.*

Received Date: 12 August 2009

Revised Date: 29 October 2009

Accepted Date: 16 November 2009



Please cite this article as: R.F. Ausas, F.S. Sousa, G.C. Buscaglia, An improved finite element space for discontinuous pressures, *Comput. Methods Appl. Mech. Engrg.* (2009), doi: [10.1016/j.cma.2009.11.011](https://doi.org/10.1016/j.cma.2009.11.011)

This is a PDF file of an unedited manuscript that has been accepted for publication. As a service to our customers we are providing this early version of the manuscript. The manuscript will undergo copyediting, typesetting, and review of the resulting proof before it is published in its final form. Please note that during the production process errors may be discovered which could affect the content, and all legal disclaimers that apply to the journal pertain.

An improved finite element space for discontinuous pressures

Roberto F. Ausas^a, Fabricio S. Sousa^{*,b}, Gustavo C. Buscaglia^b

^a*Centro Atómico Bariloche and Instituto Balseiro, 8400, Bariloche, Argentina*

^b*Instituto de Ciências Matemáticas e de Computação,
Universidade de São Paulo, 13560-970, São Carlos, Brazil*

Abstract

We consider incompressible Stokes flow with an internal interface at which the pressure is discontinuous, as happens for example in problems involving surface tension. We assume that the mesh does not follow the interface, which makes classical interpolation spaces to yield suboptimal convergence rates (typically, the interpolation error in the $L^2(\Omega)$ -norm is of order $h^{\frac{1}{2}}$). We propose a modification of the P_1 -conforming space that accommodates discontinuities at the interface without introducing additional degrees of freedom or modifying the sparsity pattern of the linear system. The unknowns are the pressure values at the vertices of the mesh and the basis functions are computed locally at each element, so that the implementation of the proposed space into existing codes is straightforward. With this modification, numerical tests show that the interpolation order improves to $\mathcal{O}(h^{\frac{3}{2}})$.

The new pressure space is implemented for the stable P_1^+/P_1 mini-element discretization, and for the stabilized equal-order P_1/P_1 discretization. As-

*Phone +55 16 33738173, Fax +55 16 33712238

Email addresses: rfausas@gmail.com (Roberto F. Ausas), fsimeoni@icmc.usp.br (Fabricio S. Sousa), gustavo.buscaglia@icmc.usp.br (Gustavo C. Buscaglia)

assessment is carried out for Poiseuille flow with a forcing surface and for a static bubble. In all cases the proposed pressure space leads to improved convergence orders and to more accurate results than the standard P_1 space. In addition, two Navier-Stokes simulations with moving interfaces (Rayleigh-Taylor instability and merging bubbles) are reported to show that the proposed space is robust enough to carry out realistic simulations.

Key words: Finite elements, interface, interpolation, discontinuous pressure, surface tension

1. Introduction

Though much progress has been made over the last years in the field of finite-element-based computational fluid mechanics, the accurate simulation of flows with significant surface tension effects remains a challenge. This is a consequence of two main difficulties that are inherent to such flows:

- (i) The surface tension force F_Γ is a surface Dirac distribution over the interface Γ , proportional to the curvature of Γ . The singularity of the force, together with its dependence of second derivatives of the interface shape, renders it difficult to approximate.
- (ii) Some of the flow variables, most importantly the pressure, are discontinuous across Γ . This leads to suboptimal interpolation accuracy whenever the finite element interpolants are continuous across Γ .

In a recent careful study, Gross and Reusken [1, 2] (see also [3]), have shown that both of the aforementioned difficulties need to be specifically

addressed or otherwise the convergence is poor (of order $h^{\frac{1}{2}}$ in the $L^2(\Omega)$ -norm). In this article the attention is focused in difficulty (ii), for which Gross and Reusken propose to adopt an XFEM [4] enrichment of the pressure space, incorporating functions that are discontinuous at Γ , as had been also proposed by Minev *et al* [5]. With this modification, they are able to get improved convergence behavior, at the expense of the well-known pitfalls of the XFEM methodology: The ill-conditioning of the system matrix due to approximate linear dependence of the basis, and the introduction of new unknowns that depend on the location of the interface, thus requiring the code to completely rebuild the linear system structure for each interface location.

Similar considerations have been made recently by Ganesan *et al* [6]. They compare mixed finite elements with continuous and discontinuous approximations for the pressure, and end up recommending the use of meshes that follow the interface together with discontinuous pressure interpolants. Clearly, this is the only combination of classical finite elements that yields a pressure space that is discontinuous at Γ , which is the key to properly tackle difficulty (ii) above. However, in a dynamic simulation it is cumbersome and sometimes impossible to maintain the mesh aligned with the interface, so that other remedies must be sought.

In this article we introduce a novel pressure space which accommodates discontinuities at the (given) interface Γ , which is approximated by piecewise-linear segments in 2D and piecewise-planar facets in 3D. The proposed space is nothing but the classical conforming P_1 space, locally modified at those elements that are cut by the interface (which will be denoted as *interface*

elements). The modification is local, computed element-by-element, and it does not introduce any additional degrees of freedom. It is thus extremely easy to incorporate the proposed space into existing codes. Further, the only discontinuities take place at Γ , so that no special treatment is needed at other interfaces (such as element-to-element interfaces, for example, as happens with Discontinuous Galerkin methods).

The proposed pressure space will be introduced in the framework of the (two-dimensional for simplicity) problem

$$-\mu \nabla^2 u + \nabla p = F_\Gamma \quad \text{in } \Omega \quad (1)$$

$$\nabla \cdot u = 0 \quad \text{in } \Omega \quad (2)$$

$$u = 0 \quad \text{on } \partial\Omega \quad (3)$$

where $F_\Gamma = f \delta_\Gamma \mathbf{n}$, with f a given function, δ_Γ the Dirac delta distribution on the line Γ , and \mathbf{n} its normal. The singular force F_Γ acts in fact as a jump condition on the normal stress across Γ , namely,

$$\left[\left[-p + 2\mu \frac{\partial u_n}{\partial n} \right] \right] = f, \quad (4)$$

whereas both the velocity and the tangential stress remain continuous. In fact, in this constant-viscosity case the velocity gradient exhibits no jump across Γ [2], so that (4) reduces to $\llbracket p \rrbracket = -f$. Notice that this simplified model also represents the so-called *actuator-disk model* that is very popular in the analysis of rotors (propellers, wind turbines, etc.) [7, 8, 9, 10, 11].

Denoting by $V = H_0^1(\Omega) \times H_0^1(\Omega)$ and $Q = L^2(\Omega)/\mathbb{R}$, the variational formulation that corresponds to (1)-(3) reads: “Find $(u, p) \in V \times Q$ such that

$$\int_{\Omega} [\mu(\nabla u + \nabla^T u) : \nabla v - p \nabla \cdot v + q \nabla \cdot u] \, d\Omega = \int_{\Gamma} f \mathbf{n} \cdot v \, d\Gamma \quad (5)$$

for all $(v, q) \in V \times Q$. The bilinear and linear forms associated to the variational formulation will be denoted by $B(\cdot, \cdot)$ and $L(\cdot)$, so that (5) can be rewritten as

$$B((u, p), (v, q)) = L(v, q). \quad (6)$$

Under reasonable regularity assumptions on Γ and f this problem admits a unique solution, since it is only necessary that L be a bounded linear functional. The finite element discretization of (5) is briefly recalled in Section 2, together with the description of the proposed pressure space. Section 3 contains several numerical experiments that assess the advantages of the proposed space with respect to classical spaces. Some conclusions are finally drawn in Section 4.

2. Finite element approximation

2.1. Galerkin mini-element formulation

In the Galerkin formulation, the exact variational formulation is restricted to the space $V_h \times Q_h$, where $V_h \subset V$ and $Q_h \subset Q$ are the approximation spaces for velocity and pressure, respectively. The discrete formulation thus reads “Find $(u_h, p_h) \in V_h \times Q_h$ such that

$$B((u_h, p_h), (v_h, q_h)) = L(v_h, q_h) \quad (7)$$

for all $(v_h, q_h) \in V_h \times Q_h$ ”. As is well-known, for this formulation to be well-posed and convergent it is sufficient that the Babuška-Brezzi stability condition [12, 13] be satisfied:

$$\inf_{q_h \in Q_h} \sup_{v_h \in V_h} \frac{\int_{\Omega} q_h \nabla \cdot v_h \, d\Omega}{\|q_h\|_Q \|v_h\|_V} \geq \beta > 0 \quad (8)$$

with β a mesh-independent constant.

The pressure and velocity spaces that correspond to the so-called mini-element [14] are, for a finite element mesh \mathcal{T}_h :

$$Q_h = Q_h^1 := \{q_h \in Q \cap \mathcal{C}^0(\Omega), q_h|_K \in P_1(K), \forall K \in \mathcal{T}_h\} \quad (9)$$

$$V_h = V_h^{\text{mini}} := \{v_h \in V, v_h|_K \in (P_1(K) \oplus \text{span}(b_K))^2, \forall K \in \mathcal{T}_h\} \quad (10)$$

where b_K is the cubic bubble function that vanishes on all three edges of K . Notice that the pressure space is nothing but the usual continuous P_1 space, while the space for each velocity component has been enriched by the bubble functions so as to satisfy the stability condition. Being stable, this element satisfies the a priori estimate

$$\|u - u_h\|_V + \|p - p_h\|_Q \leq C \left(\inf_{w_h \in V_h} \|u - w_h\|_V + \inf_{r_h \in Q_h} \|p - r_h\|_Q \right) \quad (11)$$

where C does not depend on the mesh size h . In the case of a smooth solution, there exists a constant c such that $\inf_{w_h \in V_h} \|u - w_h\|_V \leq ch |u|_{H^2(\Omega)}$ whereas $\inf_{r_h \in Q_h} \|p - r_h\|_Q \leq ch^2 |p|_{H^2(\Omega)}$. In the case of non-smooth solutions involving pressure jumps, however, the latter interpolation estimate deteriorates significantly [2], to

$$\inf_{r_h \in Q_h} \|p - r_h\|_Q \leq C \left(h^{\frac{1}{2}} \|[[p]]\|_{L^\infty(\Gamma)} + h^2 \|p\|_{H^2(\Omega \setminus \Gamma)} \right)$$

This approximation error of order $h^{\frac{1}{2}}$ is a direct consequence of the pressure interpolants being continuous *across* Γ , so that switching to discontinuous-pressure elements does not cure it, unless the mesh follows the interface.

2.2. A discontinuous pressure space with the same unknowns

The proposed variant of the mini-element combines the velocity space V_h^{mini} (Eq. 10) with a new pressure space Q_h^Γ discussed below, without any

modification of the Galerkin formulation (7).

2.2.1. The finite element interpolant

Let us now propose a different finite element space, denoted by Q_h^Γ , which has the same unknowns as the conforming P_1 space Q_h^1 but admits discontinuities across Γ . For all elements not cut by Γ standard P_1 interpolants are chosen. The only modifications appear in interface elements.

Consider the triangle ABC , which is cut by Γ into subtriangle APQ and subquadrilateral $BCQP$ (see Fig. 1). We assume for simplicity that, locally, Γ is approximated by linear segments (this would probably add an additional error of order h^2 , much smaller than the other errors involved). Let p_A, p_B, p_C denote the nodal values of the discrete pressure p_h , to be interpolated in the triangle ABC .

Let us arbitrarily denote the triangle APQ the “green” side of Γ and quadrilateral $BCQP$ the “red” side. For the approximation to be discontinuous, the function p_h on the green side needs to be solely determined by the only green node, i.e., A . Similarly, p_h on the red side must depend on just p_B and p_C . To accomplish this, we simply “carry” the value at each node towards the intersection of any edge emanating from it with the interface.

In this way, on the green side of Γ , the values at P and Q will be p_A , and thus p_h will be constant:

$$p_h|_{APQ} = p_A$$

On the red side, the value at P will be p_B and the value at Q will be p_C . One can here choose either to adopt a Q_1 interpolation in $BCQP$ from these nodal values, or subdivide the quadrilateral into two triangles, BCP and CQP . In any case, since the nodal values are given, the interpolation is immediate.

For the red triangle CQP , for example, p_h will be the linear function that takes the value p_C at vertex C , the value p_C at vertex Q , and the value p_B at vertex P . Notice that this interpolation leads to p_h being discontinuous *only* at Γ , since the function p_h restricted to any edge of the triangle is uniquely determined by the values at the nodes lying at the endpoints of that edge.

As a consequence of carrying the nodal values towards the intersection of each edge with the interface, the space Q_h^Γ consists of functions with locally an oblique derivative (in the direction of the edge that happens to cross Γ at each point) equal to zero. The interpolation error $\|p - I_h p\|_Q$ is thus expected to be of order $h^{\frac{3}{2}}$ for arbitrary $p \in W^{1,\infty}(\Omega \setminus \Gamma)$.

Remark: It could be interesting to modify the proposed space in such a way as to obtain an interpolation order of h^2 for functions with any derivative at Γ . A suitable way to do this would be by extrapolation along the edge using some recovered gradient at the nodes. This is an operation that cannot be carried out at the element level alone, and has not been explored in this work.

Remark: Some modifications are needed if the interface Γ ends within the domain (i.e., a *cracked* domain). Consider that the interface ends at some point T that lies between P and Q , so that the segment TQ is not contained in Γ . In this case the value of p_h at Q is computed by linearly interpolating the values p_A and p_C along the edge AC . The treatment of the intersection point P is as before, so that the interpolant is continuous at Q and discontinuous at P .

The extension of the proposed methodology to three dimensions follows the lines described above. For completeness, the basis functions are given

explicitly for the different possible cases in the paragraphs that follow.

2.2.2. Two-dimensional case: Standard interface element

Consider as before the triangle ABC , which is cut by Γ into the “green” subtriangle APQ and the “red” subtriangles BCP and CQP . The basis functions N_A , N_B and N_C are defined to be piecewise affine inside each of these subtriangles. It only remains to define their values at the vertices of the subtriangles, i.e., at the points A , B , C , P and Q . However, since they are discontinuous at Γ , two values are given at points P and Q . The values on the green side will be assigned a “plus” sign, while those on the red side a “minus” sign. The values at the vertices are:

$$N_A(A) = 1 \quad N_B(A) = 0 \quad N_C(A) = 0 \quad (12)$$

$$N_A(B) = 0 \quad N_B(B) = 1 \quad N_C(B) = 0 \quad (13)$$

$$N_A(C) = 0 \quad N_B(C) = 0 \quad N_C(C) = 1 \quad (14)$$

$$N_A(P^+) = 1 \quad N_B(P^+) = 0 \quad N_C(P^+) = 0 \quad (15)$$

$$N_A(P^-) = 0 \quad N_B(P^-) = 1 \quad N_C(P^-) = 0 \quad (16)$$

$$N_A(Q^+) = 1 \quad N_B(Q^+) = 0 \quad N_C(Q^+) = 0 \quad (17)$$

$$N_A(Q^-) = 0 \quad N_B(Q^-) = 0 \quad N_C(Q^-) = 1 \quad (18)$$

Notice that these functions satisfy several useful properties: (i) They form a nodal basis, in the sense that they take the value one at their corresponding node and zero at the other nodes; (ii) their sum equals the constant function equal to one in K ; (iii) their extreme values (zero and one) take place at the nodes. A picture of the interpolation functions for this case can be seen on Fig. 2.

Remark: Though unlikely in practical cases, it could happen that Γ passes exactly through a vertex. This is a degenerate case in which one of the subtriangles becomes a needle of vanishingly small volume.

2.2.3. Two-dimensional case: Element containing an interface endpoint

In the case that Γ has an endpoint at element K , special basis functions are needed. Consider P to be the last edge-interface intersection point, and T to be the interface endpoint (see Figure 3). The point Q is defined as the intersection of the line PT with the edge AC . The difference with the previous case is that now the functions need to be continuous at point Q .

For this purpose, let g be an affine function defined on the edge AC such that $g(A) = 1$ and $g(C) = 0$ (in other words, g is the restriction to edge AC of the P_1 basis function corresponding to node A). The values of N_A , N_B and N_C at points A , B , C , P^+ and P^- are as in (12)-(16). At point Q the functions are continuous, with values

$$N_A(Q) = g(Q), \quad N_B(Q) = 0, \quad N_C(Q) = 1 - g(Q) \quad (19)$$

Properties (i)-(iii) above are also satisfied by this basis. An illustration of these functions can be seen on Fig. 4.

2.2.4. Three-dimensional case: Standard interface element

Consider that the element K cut by the interface is the tetrahedron $ABCD$ as shown in Fig. 5, of which either three (case (a)) or four (case (b)) edges are cut by Γ .

In case (a), there appear three intersection points P , Q and R (see Fig. 5(a)), at which the nodal functions N_A , N_B , N_C and N_D are bi-valued. As

in the two-dimensional case, the plus and minus values at the intersection points correspond to the “green” and “red” sides of the interface. Carrying the values to the interface as explained, the values of the basis functions at the vertices and intersection points are:

$$N_A(A) = 1, \quad N_B(A) = 0, \quad N_C(A) = 0, \quad N_D(A) = 0 \quad (20)$$

$$N_A(B) = 0, \quad N_B(B) = 1, \quad N_C(B) = 0, \quad N_D(B) = 0 \quad (21)$$

$$N_A(C) = 0, \quad N_B(C) = 0, \quad N_C(C) = 1, \quad N_D(C) = 0 \quad (22)$$

$$N_A(D) = 0, \quad N_B(D) = 0, \quad N_C(D) = 0, \quad N_D(D) = 1 \quad (23)$$

$$N_A(P^+) = 1, \quad N_B(P^+) = 0, \quad N_C(P^+) = 0, \quad N_D(P^+) = 0 \quad (24)$$

$$N_A(P^-) = 0, \quad N_B(P^-) = 1, \quad N_C(P^-) = 0, \quad N_D(P^-) = 0 \quad (25)$$

$$N_A(Q^+) = 1, \quad N_B(Q^+) = 0, \quad N_C(Q^+) = 0, \quad N_D(Q^+) = 0 \quad (26)$$

$$N_A(Q^-) = 0, \quad N_B(Q^-) = 0, \quad N_C(Q^-) = 1, \quad N_D(Q^-) = 0 \quad (27)$$

$$N_A(R^+) = 1, \quad N_B(R^+) = 0, \quad N_C(R^+) = 0, \quad N_D(R^+) = 0 \quad (28)$$

$$N_A(R^-) = 0, \quad N_B(R^-) = 0, \quad N_C(R^-) = 0, \quad N_D(R^-) = 1 \quad (29)$$

The truncated tetrahedron $BCDPQR$ is divided into subtetrahedra and from the values at the vertices given above the basis functions are obtained by affine interpolation over each subtetrahedron. Satisfaction of 3D analogs of properties (i)-(iii) is straightforward. In this case, for the resulting interpolant not to be discontinuous at the faces (outside Γ) the neighbor element must be subdivided in a compatible way. For face ABC , for example, continuity of N_B and N_C is only obtained if both elements sharing this face divide the quadrilateral $BCPQ$ by the same diagonal.

In case (b) there appear four intersection points, namely P , Q , R and

S (see Fig. 5(b)). The values of the basis functions at A , B , C and D are obviously the same as in (20)-(23). The values at the intersection points follow the same procedure as before, yielding

$$N_A(P^+) = 1, \quad N_B(P^+) = 0, \quad N_C(P^+) = 0, \quad N_D(P^+) = 0 \quad (30)$$

$$N_A(P^-) = 0, \quad N_B(P^-) = 0, \quad N_C(P^-) = 1, \quad N_D(P^-) = 0 \quad (31)$$

$$N_A(Q^+) = 1, \quad N_B(Q^+) = 0, \quad N_C(Q^+) = 0, \quad N_D(Q^+) = 0 \quad (32)$$

$$N_A(Q^-) = 0, \quad N_B(Q^-) = 0, \quad N_C(Q^-) = 0, \quad N_D(Q^-) = 1 \quad (33)$$

$$N_A(R^+) = 0, \quad N_B(R^+) = 1, \quad N_C(R^+) = 0, \quad N_D(R^+) = 0 \quad (34)$$

$$N_A(R^-) = 0, \quad N_B(R^-) = 0, \quad N_C(R^-) = 1, \quad N_D(R^-) = 0 \quad (35)$$

$$N_A(S^+) = 0, \quad N_B(S^+) = 1, \quad N_C(S^+) = 0, \quad N_D(S^+) = 0 \quad (36)$$

$$N_A(S^-) = 0, \quad N_B(S^-) = 0, \quad N_C(S^-) = 0, \quad N_D(S^-) = 1 \quad (37)$$

Properties (i)-(iii) are easily seen to hold, while continuity across the faces again depends on the compatibility of the subdivisions between neighboring elements.

2.2.5. Three-dimensional case: Interface with boundary

If the interface Γ has a boundary $\partial\Gamma$ within the domain, the basis functions need to be modified in much the same way as in the two-dimensional case. Let K be an element cut by the surface Γ and such that $\partial\Gamma \cap K \neq \emptyset$. We assume that $\Gamma \cap K$ is a planar polygon and thus the intersection of this plane with the edges of K defines the points P , Q , R and, in a case-(b) situation, S , as before.

Consider for example that the intersection is as shown in Fig. 6, so that the subdivision corresponds to case (b). Notice, however, that the edge

BD is not crossed by the interface, so that the basis functions must be continuous along this edge and thus, in particular, at point S . Proceeding as in the two-dimensional case, we assign to S a unique value provided by the linear interpolation between nodes B and D . This procedure is adopted for all intersection points falling outside Γ . Properties (i)-(iii) are easily seen to hold, as well as continuity of the basis functions across the faces (again depending on a compatible choice of diagonals for quadrilaterals).

2.3. A stabilized method

It is also possible to consider finite element formulations that do not satisfy the Babuška-Brezzi condition (8), but are rendered convergent by means of stabilization techniques [15, 16]. This is the case of the equal-order P_1/P_1 formulation in which the discrete spaces are

$$Q_h = Q_h^1 \quad (\text{as before}) \quad (38)$$

$$V_h = V_h^1 := \{v_h \in V, v_h|_K \in P_1(K)^2, \forall K \in \mathcal{T}_h\} \quad (39)$$

and the formulation reads: “Find $(u_h, p_h) \in V_h \times Q_h$ such that

$$B((u_h, p_h), (v_h, q_h)) + \sum_{K \in \mathcal{T}_h} \tau_K \int_K \mathcal{R}(u_h, p_h) \cdot \nabla q_h \, dK = L(v_h, q_h) \quad (40)$$

for all $(v_h, q_h) \in V_h \times Q_h$ ”. The stabilization coefficient τ_K is taken as

$$\tau_K = \frac{h_K^2}{4\mu}$$

where h_K is the element size, and the residual is defined as

$$\mathcal{R}(u_h, p_h) = -\mu \nabla^2 u_h + \nabla p_h - F_\Gamma. \quad (41)$$

For regular forces (e.g., forces in $L^2(\Omega)$, which is not the case of F_Γ), it is possible to prove an error estimate [16] which is essentially equivalent to (11).

To our knowledge, no analysis exists of stabilized methods in problems involving singular forces. Our approach is to set τ_K to zero whenever the element K is cut by the interface. Though this could potentially lead to lack of stability, no spurious pressure modes were detected in any of the numerical tests. We attribute this to the band-like structure of the submesh in which the stabilization is omitted, which is too narrow (just one band of elements) for spurious modes to develop. In a different context, Lew and Buscaglia [17] observed that switching the elements crossed by Γ to a discontinuous Galerkin discretization required no stabilization, *though the same space indeed requires stabilization when used in the whole domain.*

3. Numerical experiments

In this section we carry out numerical assessments of the proposed space. We first investigate the interpolation accuracy of the space Q_h^Γ and indeed obtain the claimed $h^{\frac{3}{2}}$ -order in the $L^2(\Omega)$ -norm. Then we turn to academic Navier-Stokes tests with analytic solution in which Q_h^Γ is used as pressure space. These tests show that the new space does not deteriorate the stability properties of either the stable mini-element formulation or the stabilized equal-order formulation. Finally, two more realistic problems are simulated to show that the proposed method is robust enough to handle arbitrarily moving interfaces in two and three dimensions.

3.1. Interpolation properties of the space Q_h^Γ

We first assess purely the interpolation properties of Q_h^Γ . For this purpose we perform tests similar to those conducted by Reusken [3]. Let $\Omega = (-\frac{\pi}{2}, \frac{\pi}{2}) \times (-\frac{\pi}{2}, \frac{\pi}{2})$ and let $\Gamma = \{(x, y) \in \Omega \mid x = 0, y > 0\}$. Let p be the function

$$p(x, y) = \begin{cases} e^{-x} \sin^2(y) & \text{if } (x > 0 \text{ and } y > 0) \\ 0 & \text{otherwise} \end{cases}. \quad (42)$$

Notice that Γ is a “crack” in the domain, and that p is discontinuous across Γ .

The interpolant $\mathcal{I}_h p$ of p is now defined as the unique element of Q_h^Γ that coincides with p at all the vertices of \mathcal{T}_h .

A sequence of unstructured meshes was built, of which the first one is shown in Fig. 7. To this mesh, which consists of 326 triangles, we assign a mesh size of $h = 0.2$. The following meshes in the sequence are built by successively dividing each of the triangles of the previous mesh into four equal triangles, leading to meshes with $h = 0.1$, $h = 0.05$ and so forth, until the finest mesh with $h = 3.125 \times 10^{-3}$.

We measured the error of $p - \mathcal{I}_h p$ in the $L^2(\Omega)$ -norm. The results are shown in Table 1, in which we also include the interpolation error of the P_1 -conforming interpolant for comparison (Q_h^1). Figure 8 displays the convergence rate of the order of $h^{\frac{3}{2}}$.

3.2. Couette flow

In this experiment we consider the domain $[0, L] \times [0, H]$, with periodic boundary conditions in the x_1 -direction. The velocity is set to zero at the

top and bottom boundaries

$$u(x_1, x_2 = 0) = u(x_1, x_2 = H) = 0$$

and the interface Γ is a straight vertical line $x_1 = a$, on which a constant unit normal force $f = 1$ is imposed. The exact solution for this problem is

$$u_1(x_1, x_2) = \frac{1}{2\mu L} x_2 (H - x_2) \quad (43)$$

$$u_2(x_1, x_2) = 0 \quad (44)$$

$$p(x_1, x_2) = -\frac{1}{L} x_1 + \mathcal{H}(x_1 - a) \quad (45)$$

where $\mathcal{H}(x_1 - a) = 1$ if $x_1 > a$ and zero otherwise, and the indeterminacy of the pressure was removed by imposing $p(0, 0) = 0$ instead of setting the average to zero, for simplicity.

This problem, with $L = 3$, $H = 1$, $\mu = 1$ and $a = 2$ was discretized both with the mini-element and with the stabilized equal-order methods. In both cases, the classical P_1 -conforming pressure space (denoted by Q_h^1 above) and the new space Q_h^Γ were implemented.

As in the previous section, a sequence of unstructured meshes was built, of which the first one is shown in Fig. 9. To this mesh, which consists of 220 triangles, we assign a mesh size of $h = 0.176$. The following meshes in the sequence are built by subdivision. We measure the velocity error in the $H^1(\Omega)$ -norm and the pressure error in the $L^2(\Omega)$ -norm for both methods as functions of h . The results of the convergence analysis are displayed in Table 2 and Fig. 10. The experimental orders of convergence are

$$\|u - u_h\|_{H^1(\Omega)} = \mathcal{O}(h^{\frac{1}{2}}), \quad \|p - p_h\|_{L^2(\Omega)} = \mathcal{O}(h^{\frac{1}{2}})$$

for the standard Q_h^1 space; and

$$\|u - u_h\|_{H^1(\Omega)} = \mathcal{O}(h), \quad \|p - p_h\|_{L^2(\Omega)} = \mathcal{O}(h)$$

for the proposed method. The optimal convergence of smooth problems is thus recovered with the proposed modification of the pressure space.

The pressure field corresponding to the classical mini-element is compared to that obtained with the proposed method in Fig. 11. As is clear from the figure, the improved pressure space exhibits significantly smaller pressure oscillations near the interface than the mini-element.

3.3. Static two-dimensional bubble

The second example we report here concerns a 2D static bubble. In this case the interface Γ is the circle of radius R centered at the origin. On Γ , a constant (inwards) normal force is imposed, $f = \frac{\sigma}{R}$, where σ represents the surface tension. Setting the pressure outside the bubble arbitrarily to zero, the exact pressure inside the bubble equals $\frac{\sigma}{R}$. The exact velocity vanishes everywhere.

In this example we approximate Γ by Γ_h , which consists of straight segments inside each element that join the intersections of Γ with the element edges (i.e., the points P and Q are joined by a straight segment). With Γ_h fixed, we impose the surface tension force in two ways:

Direct forcing: We impose

$$F_\Gamma = -\frac{\sigma}{R} \delta_{\Gamma_h} \mathbf{e}_r \quad (46)$$

where \mathbf{e}_r is the radial unit vector, leading to

$$L(v_h, q_h) = -\frac{\sigma}{R} \int_{\Gamma_h} \mathbf{e}_r \cdot v_h \, d\Gamma \quad (47)$$

Laplace-Beltrami forcing: The Laplace-Beltrami treatment of surface tension is based on the identity (valid for a closed surface of curvature κ)

$$\int_{\Gamma} \kappa \mathbf{n} \cdot v \, d\Gamma = - \int_{\Gamma} (\mathbb{I} - \mathbf{n} \otimes \mathbf{n}) : \nabla v \, d\Gamma \quad (48)$$

where \mathbb{I} is the identity tensor, the symbol \otimes denotes the tensor product, and “:” stands for the double contraction of rank two tensors. This leads to the following linear form on the right-hand side of (7) and/or (40):

$$L(v_h, q_h) = - \sigma \int_{\Gamma_h} (\mathbb{I} - \mathbf{n}_h \otimes \mathbf{n}_h) : \nabla v_h \, d\Gamma \quad (49)$$

where \mathbf{n}_h is the unit normal to Γ_h .

For the numerical tests we chose $R = \mu = \sigma = 1$, and the domain was set to $\Omega = (-2, 2) \times (-2, 2)$. The velocity is set to zero on $\partial\Omega$, and the pressure at the left bottom corner of the domain is set to zero to fully determine the pressure. We present results for the mini-element formulation with direct forcing (ME+DF), and for the stabilized formulation with Laplace-Beltrami forcing (ST+LB). A mesh refinement study was conducted in the same way as in the previous examples, starting with the mesh shown in Fig. 12, to which we assign $h = 0.2$. Logarithmic plots of the velocity and pressure errors are shown in Fig. 13. Clearly, both methods converge with order $\mathcal{O}(h^{\frac{1}{2}})$ if the standard pressure space Q_h^1 is used, while switching to Q_h^Γ improves the order to $\mathcal{O}(h^{\frac{3}{2}})$. The obtained pressure and velocity fields on the mesh with $h = 0.05$, which consists of 14900 elements, are shown in Figs. 14 and 15 for the ME+DF formulation, and in Figs. 16 and 17 for the ST+LB formulation. The improvements brought by the proposed method are evident. The parasitic velocities obtained with the ME+DF formulation have

a maximum modulus of 1.6×10^{-3} when the P_1 space is used for pressure, whereas with the proposed space this value is much smaller (4.5×10^{-5}). Similarly, in the ST+LB formulation the maximum velocity modulus is 2.4×10^{-3} for Q_h^1 and 7×10^{-5} for Q_h^F .

3.4. Rayleigh-Taylor instability

This is a well-known benchmark which has been computed by Puckett *et al* [18], Popinet and Zaleski [19] and Jahanbakhsh *et al* [20], among others. It consists of a layer of heavier fluid ($\rho = 1.225$) on top of a lighter fluid ($\rho = 0.1694$), both with viscosity $\mu = 3.13 \times 10^{-2}$. The domain is the rectangle $\Omega = (0, 1) \times (0, 4)$ and the gravity is taken as $g = 10$. The interface between the fluids is a horizontal line with a sinusoidal perturbation of amplitude 0.05. We consider the standard case, with no surface tension, and also simulate a case with $\sigma = 0.025$ in which the ability of the numerical method to reproduce the stabilizing effect of surface tension is tested.

To carry out this simulation (and the one in the next subsection) the proposed pressure space was incorporated into a general purpose in-house interface-capturing code that simulates fluids with evolving interfaces. The details of the code are explained elsewhere [21]. Let us here simply summarize its basic ingredients:

- Stabilized equal-order formulation of the time-dependent Navier-Stokes equations.
- Level set formulation for interface representation and transport. Standard P_1 conforming elements for the level set function ϕ . The transport

of ϕ is handled with the SUPG method [22], with mass-preserving periodic reinitialization as proposed by Mut *et al* [23].

- Laplace-Beltrami treatment of the surface tension force.

Numerical results at several times, as computed on a uniform mesh consisting of 331,776 elements with a time step $\Delta t = 6.25 \times 10^{-4}$ are shown in Fig. 18. The results with $\sigma = 0$ are in good agreement with those reported by Jahanbakhsh *et al* [20], while the stabilizing effect of surface tension is clear from the simulation results with $\sigma = 0.025$.

3.5. Merging bubbles

This experiment shows the good behavior of the proposed method in three-dimensional complex cases. We study the rise of two buoyant bubbles ($\rho = 0.04$, $\mu = 5 \times 10^{-3}$) in a quiescent liquid with $\rho = 1$ and $\mu = 0.1$. The diameter of the bubbles is 1 and the domain is $\Omega = (0, 3) \times (0, 3) \times (0, 4)$. The gravity is $g = 10$, the surface tension $\sigma = 0.2$ and the initial positions of the bubbles' centers are $(1.5, 1.5, 2.25)$ and $(1.5, 1.75, 1)$ (notice that they are not vertically aligned).

The finite element mesh consists of 885,000 tetrahedra, and the time step is taken as 10^{-3} . Shown in Fig. 19 is the interface shape at times $t = 0.125$, 0.25, 0.35, 0.4, 0.5 and 0.575. The bottom bubble follows and catches the top one, and the results are in good agreement with those reported by Sousa *et al* [24] and Marchandise *et al* [25].

4. Conclusions

A new finite element space Q_h^Γ has been proposed, which has the same unknowns as the P_1 -conforming space but consists of functions that are discontinuous across a given interface Γ , assumed not aligned with the mesh. The proposed space is much simpler than the one proposed by Gross and Reusken [2], which is based on XFEM enrichment, and also to the one proposed by Fries and Belytschko [26], which avoids introducing additional unknowns by switching to a moving-least-squares approximation in the vicinity of Γ .

Through numerical tests it was shown that the $L^2(\Omega)$ -interpolation accuracy of Q_h^Γ for functions that are smooth outside Γ is $\mathcal{O}(h^{\frac{3}{2}})$. This is a significant improvement with respect to the accuracy of continuous spaces of any polynomial degree, which is $\mathcal{O}(h^{\frac{1}{2}})$.

An interpolation accuracy of $\mathcal{O}(h^{\frac{3}{2}})$ in the $L^2(\Omega)$ -norm is suboptimal for piecewise linear elements. However, the a priori estimate (11) implies that the space Q_h^Γ , when taken as pressure space, will *not* limit the accuracy of a (Navier-)Stokes calculation neither in equal-order velocity-pressure approximations, nor in the mini-element approximation. In fact, in both cases the global accuracy is limited by the $H^1(\Omega)$ -accuracy of the velocity space, which is $\mathcal{O}(h)$.

The proposed space is easy to implement, requiring just local operations at the element level to incorporate the improved pressure interpolation. Several tests were reported which illustrate the improved behavior of both velocity and pressure when the elements cut by the interface are treated with the proposed pressure interpolants.

Some issues are left for future work. A rigorous proof of the interpolation

estimate has been undertaken by Agouzal and Buscaglia, of which some preliminary results have already been communicated [27] and a complete version is in preparation. Another open theoretical question concerns the stability estimates for the $V_h-Q_h^\Gamma$ pair, of which strong numerical evidence has been provided in this article but whose proof is far from evident. Finally, it would be interesting to devise spaces analog to Q_h^Γ when the overall discretization is P_k -conforming with $k > 1$, but this is, again, far from being an immediate extension of the space proposed in this article.

ACKNOWLEDGMENTS: The authors acknowledge partial support from FAPESP (Brazil), CNPq (Brazil), CNEA (Argentina) and CONICET (Argentina). This research was carried out in the framework of INCT-MACC, Ministério de Ciência e Tecnologia, Brazil.

References

- [1] S. Gross and A. Reusken. Finite element discretization error analysis of a surface tension force in two-phase incompressible flows. *SIAM J. Numer. Anal.*, 45:1679–1700, 2007.
- [2] S. Gross and A. Reusken. An extended pressure finite element space for two-phase incompressible flows with surface tension. *Journal of Computational Physics*, 224:40–58, 2007.
- [3] A. Reusken. Analysis of an extended pressure finite element space for two-phase incompressible flows. *Comput. Visual. Sci.*, 11:293–305, 2008.
- [4] T. Belytschko, N. Moës, S. Usui, and C. Parimi. Arbitrary disconti-

- nities in finite elements. *Int. J. Numer. Meth. Engng*, 50:993–1013, 2001.
- [5] P.D. Minev, T. Chen, and K. Nandakumar. A finite element technique for multifluid incompressible flow using Eulerian grids. *Journal of Computational Physics*, 187:225–273, 2003.
- [6] S. Ganesan, G. Matthies, and L. Tobiska. On spurious velocities in incompressible flow problems with interfaces. *Comput. Methods Appl. Mech. Engrg.*, 196:1193–1202, 2007.
- [7] R. Mikkelsen. Actuator disc methods applied to wind turbines. Ph. D. Thesis MEK-FM-PHD 2003-02. Technical Univ. Denmark. June 2003.
- [8] C. Meyer and D. Kröger. Numerical simulation of the flow field in the vicinity of an axial flow fan. *Int. J. Numer. Meth. Fluids*, 36:947–969, 2001.
- [9] Y. Tahara, R. Wilson, P. Carrica and F. Stern. RANS simulation of a container ship using a single-phase level-set method with overset grids and the prognosis for extension to a self-propulsion simulator. *J. Marine Sci. Technol.*, 11:209–228, 2006.
- [10] P. Carrica, K.-J. Paik, H. Hosseini and F. Stern. URANS analysis of a broaching event in irregular quartering seas. *J. Marine Sci. Technol.*, 13:395–407, 2008.
- [11] C. Leclerc and C. Masson. Wind turbine performance predictions using a differential actuator–lifting disk model. *J. Solar Energy Engng.*, 127:200–208, 2005.

- [12] I. Babuška. The finite element method with Lagrangian multipliers. *Numer. Math.*, 20:179–192, 1973.
- [13] F. Brezzi. On the existence, uniqueness and approximation of saddle-point problems arising from Lagrange multipliers. *RAIRO Anal. Numér.*, 8:129–151, 1974.
- [14] D. Arnold, F. Brezzi and M. Fortin. A stable finite element for the Stokes equations. *Calcolo*, 21:337–344, 1984.
- [15] T.J.R. Hughes, L. Franca and M. Balestra. A new finite element formulation for computational fluid dynamics: V. Circumventing the Babuška-Brezzi condition. A stable Petrov-Galerkin formulation of the Stokes problem accommodating equal-order interpolations. *Comput. Methods Appl. Mech. Engrg.*, 59:85–99, 1986.
- [16] L. Franca and T.J.R. Hughes. Two classes of mixed finite element methods. *Comput. Methods Appl. Mech. Engrg.*, 69:89–129, 1988.
- [17] A. Lew and G. Buscaglia. A discontinuous-Galerkin-based immersed boundary method. *Int. J. Numer. Meth. Engng.*, 76:427–454, 2008.
- [18] E. Puckett, A. Almgren, J. Bell, D. Marcus and W. Rider. A high-order projection method for tracking fluid interfaces in variable density incompressible flows. *Journal of Computational Physics*, 130:269–282, 1997.
- [19] S. Popinet and S. Zaleski. A front-tracking algorithm for accurate representation of surface tension. *Int. J. Numer. Meth. Fluids*, 30:775–793, 1999.

- [20] E. Jahanbakhsh, R. Panahi and M. Serif. Numerical simulation of three-dimensional interfacial flows. *Int. J. Numer. Meth. Heat & Fluid Flow*, 17:384–404, 2007.
- [21] R. Ausas. *Ph. D. Thesis in Nuclear Engineering*. Instituto Balseiro, Argentina. In preparation.
- [22] A. Brooks and T.J.R. Hughes. Streamline upwind/Petrov-Galerkin formulations for convection dominated flows with particular emphasis on the incompressible Navier-Stokes equations. *Comput. Methods Appl. Mech. Engrg.*, 32:199–259, 1982.
- [23] F. Mut, G. Buscaglia and E. Dari. New mass-conserving algorithm for level set redistancing on unstructured meshes. *Journal of Applied Mechanics*, ASME, 73:1011–1016, 2006.
- [24] F.S. de Sousa, N. Mangiavacchi, L.G. Nonato, A. Castelo, M.F. Tome, V.G. Ferreira, J.A. Cuminato and S. McKee. A front-tracking/front-capturing method for the simulation of 3D multi-fluid flows with free surfaces. *Journal of Computational Physics*, 198:469–499, 2004.
- [25] E. Marchandise, P. Geuzaine, N. Chevaugeon, and J.-F. Remacle. A stabilized finite element method using a discontinuous level set approach for the computation of bubble dynamics. *Journal of Computational Physics*, 225:949–974, 2007.
- [26] T.-P. Fries and T. Belytschko. The intrinsic XFEM: a method for arbitrary discontinuities without additional unknowns. *Int. J. Numer. Meth. Engrg.*, 68:1358–1385, 2006.

- [27] G. Buscaglia and A. Agouzal. Interpolation estimate for a finite element space with embedded discontinuities. In *Proc. 30th Iberian-Latin-American Congress on Computational Methods in Engineering*, Búzios, Brazil, November 8–11, 2009.

ACCEPTED MANUSCRIPT

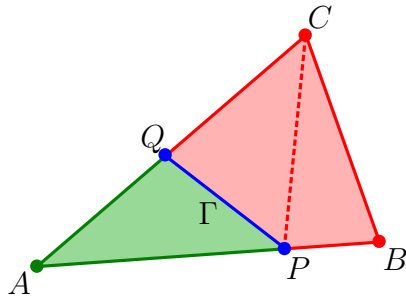


Figure 1: Partition of a single finite element into subelements following the interface PQ .

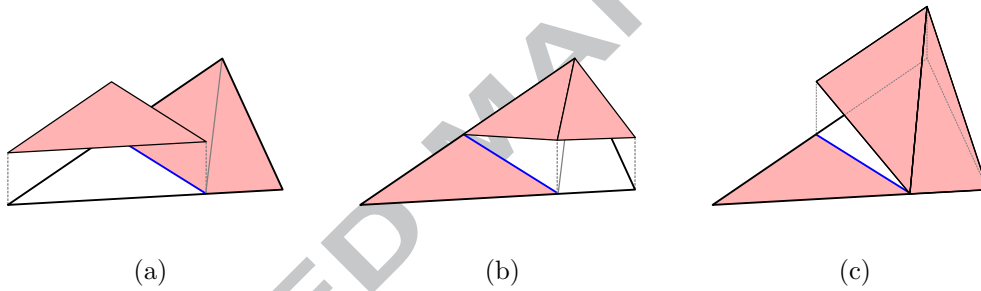


Figure 2: Basis functions for the new finite element space inside an element crossed by the interface: (a) N_A , (b) N_B and (c) N_C .

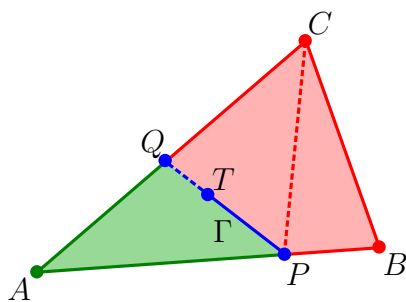


Figure 3: Endpoint T of the interface Γ inside the element ABC .

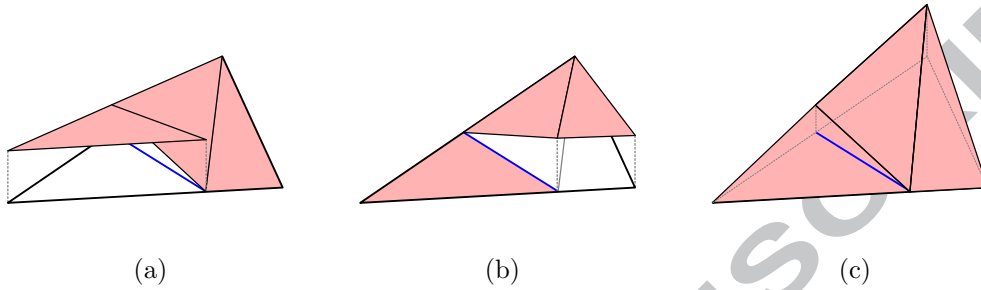


Figure 4: Basis functions for the new finite element space inside an element containing an endpoint of the interface: (a) N_A , (b) N_B and (c) N_C .

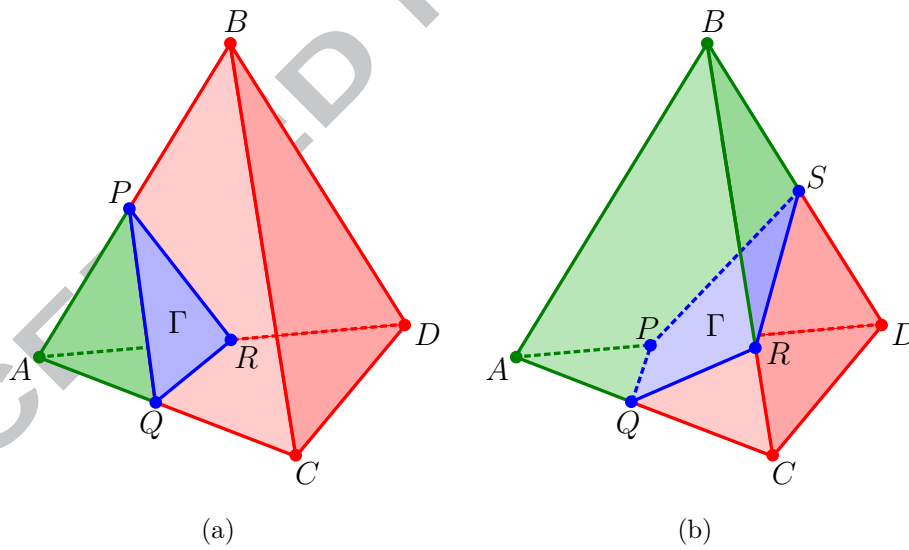


Figure 5: Partition of a tetrahedron following the interface Γ : (a) Interface crossing three edges; (b) Interface crossing four edges.

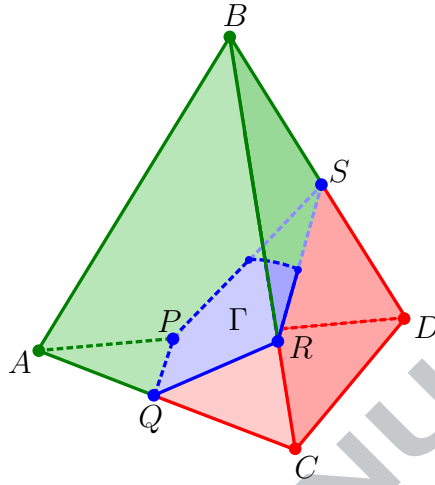


Figure 6: Partition of a tetrahedron K where $\partial\Gamma \cap K \neq \emptyset$. Point S is obtained by intersecting plane PQR with edge BD .

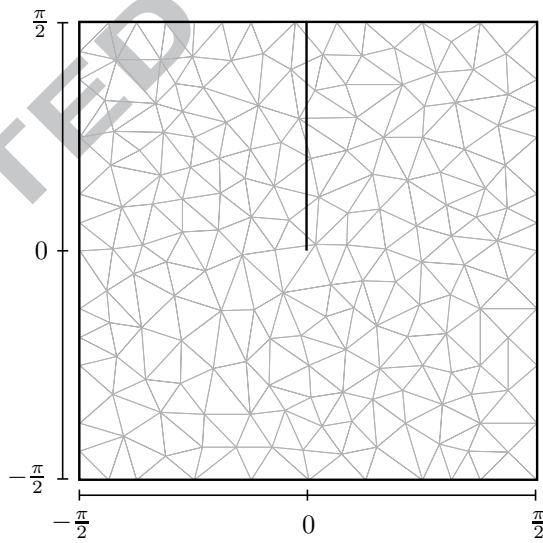


Figure 7: First mesh used in the interpolation test, with 326 elements. The interface Γ is a line from $(0,0)$ to $(0, \frac{\pi}{2})$.

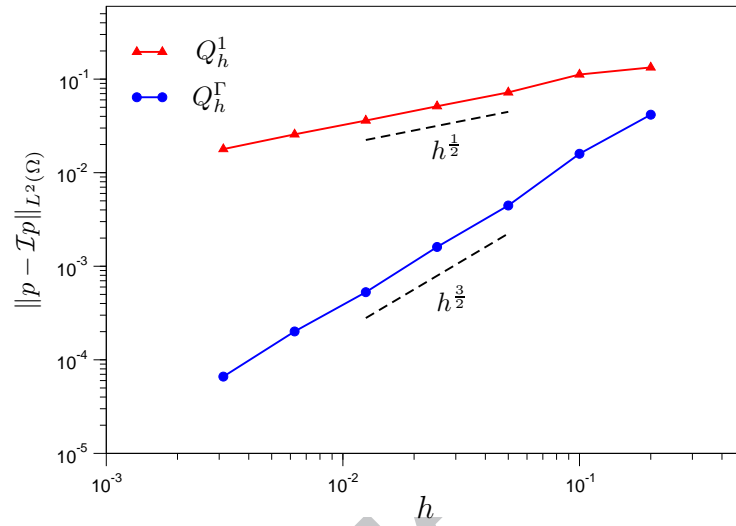


Figure 8: Convergence rate of the error in L^2 -norm for the interpolated function $p(x, y)$ using standard Q_h^1 and the new pressure space Q_h^Γ .

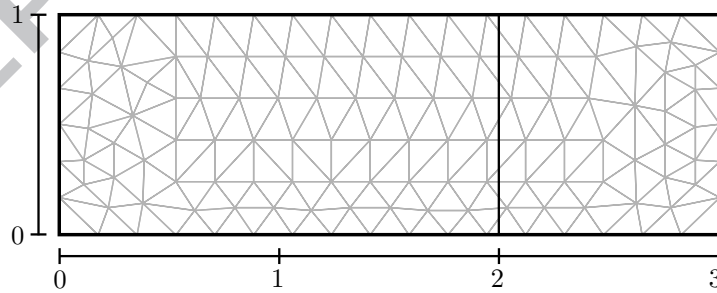
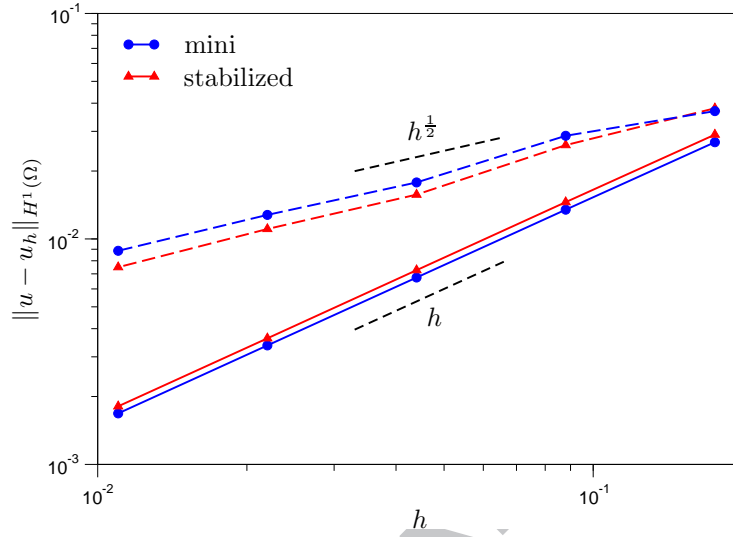
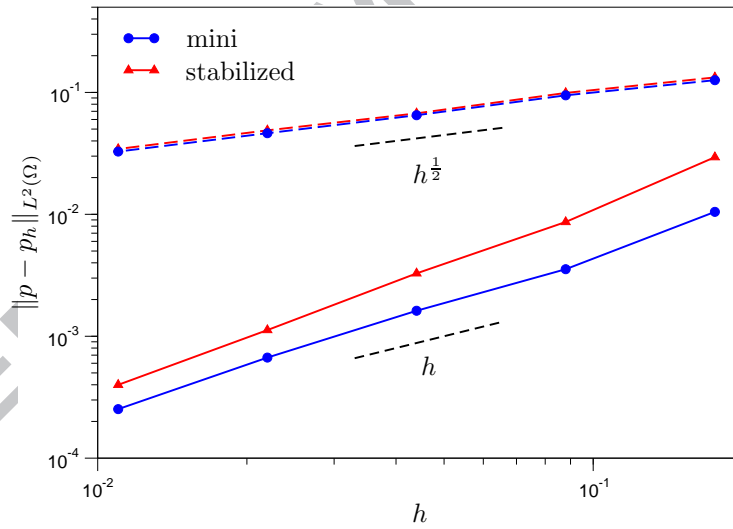


Figure 9: Mesh with 220 elements, $h = 0.176$, for the Couette convergence test.



(a)



(b)

Figure 10: Error norms for the velocity (a) and pressure (b), showing the convergence rates for the Couette flow. Dashed lines represent the standard Q_h^1 pressure interpolation and continuous lines represent the new Q_h^Γ discontinuous element.

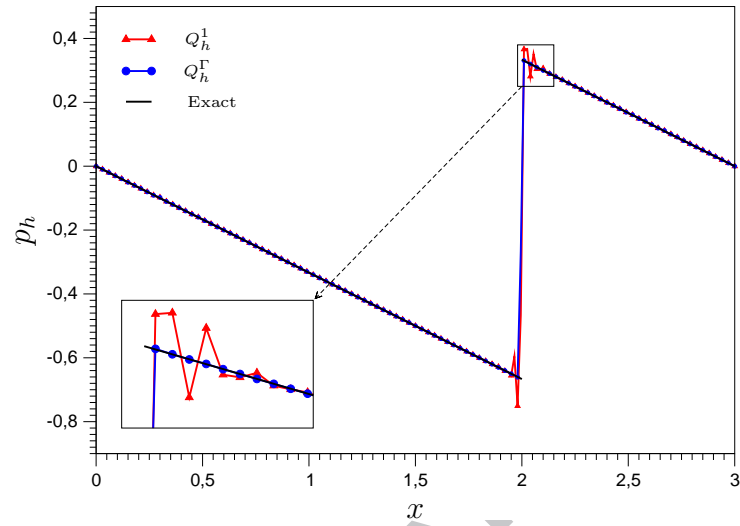


Figure 11: Computed pressure using the stable formulation (mini-element), with standard and new pressure space.

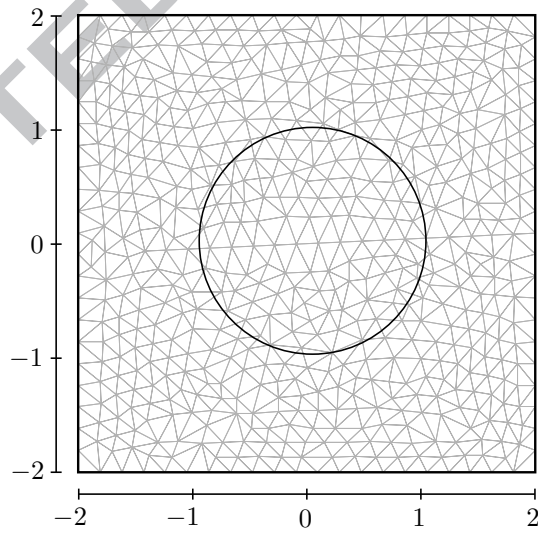
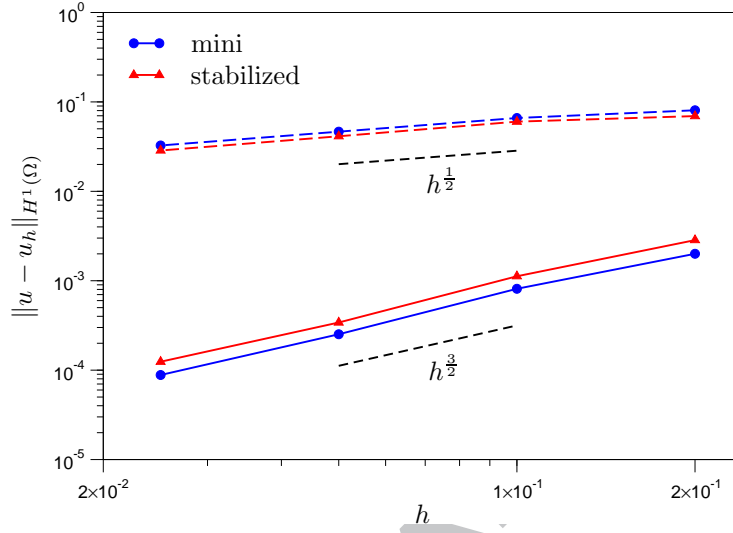
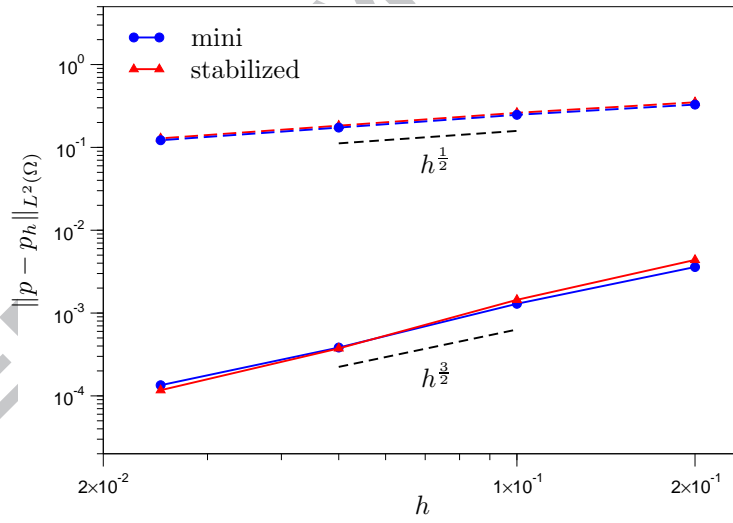


Figure 12: Mesh for the static bubble convergence study, with 1104 elements and $h = 0.2$.

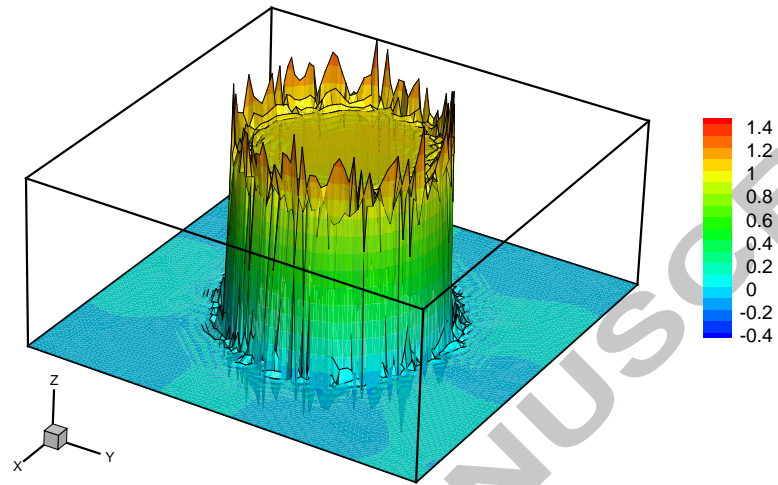


(a)

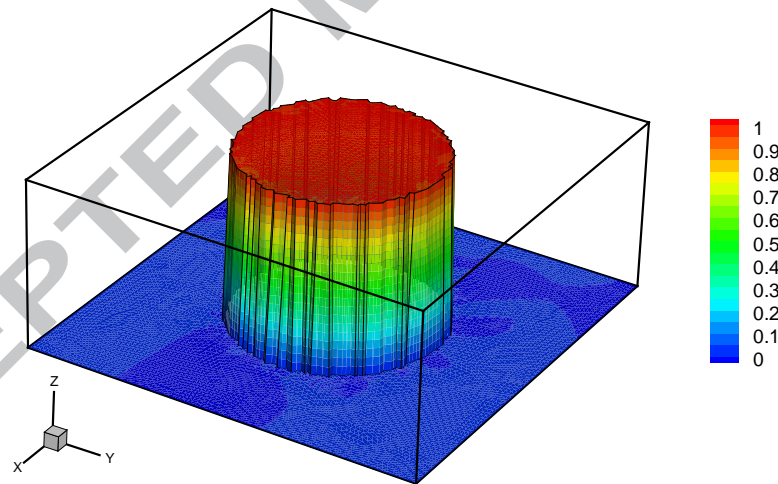


(b)

Figure 13: Error norms for the velocity (a) and pressure (b), showing the convergence rates for the static bubble. Dashed lines represent the standard Q_h^1 pressure interpolation and continuous lines represent the new Q_h^Γ discontinuous element.



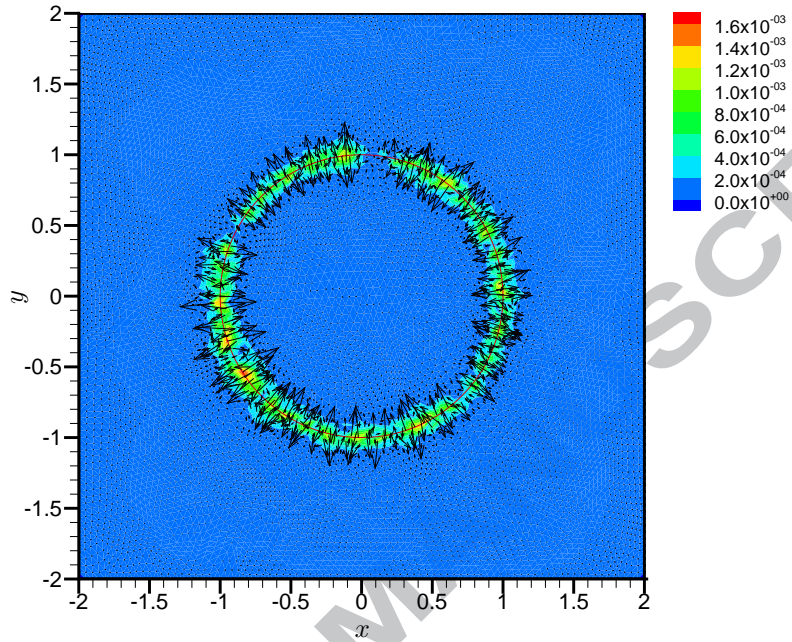
(a)



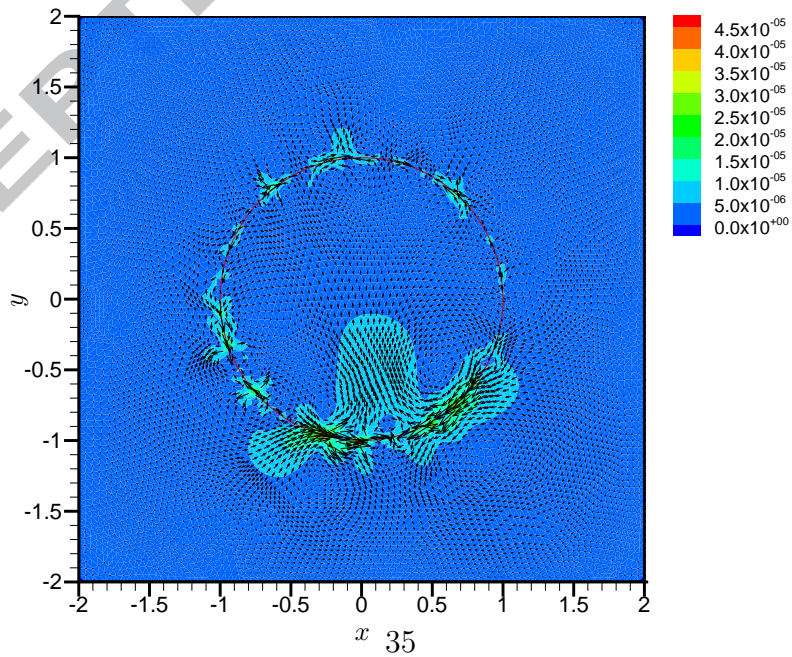
(b)

Figure 14: Pressure field for the mini-element with direct forcing, obtained with $h = 0.05$:

(a) Q_h^1 ; (b) Q_h^Γ .

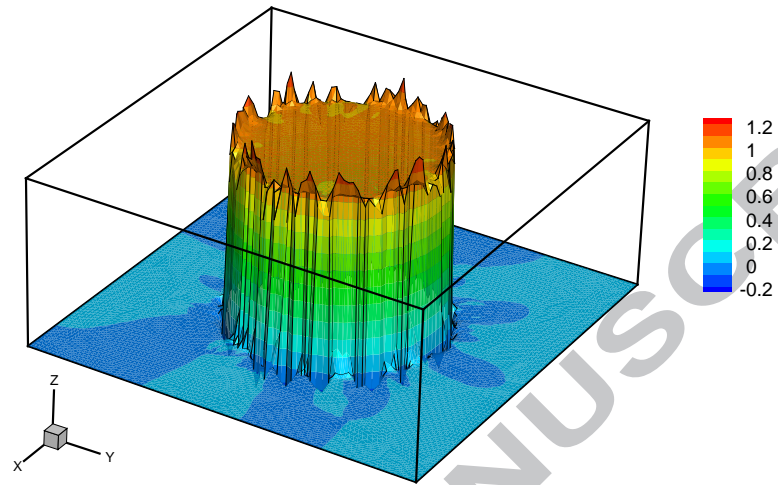


(a)

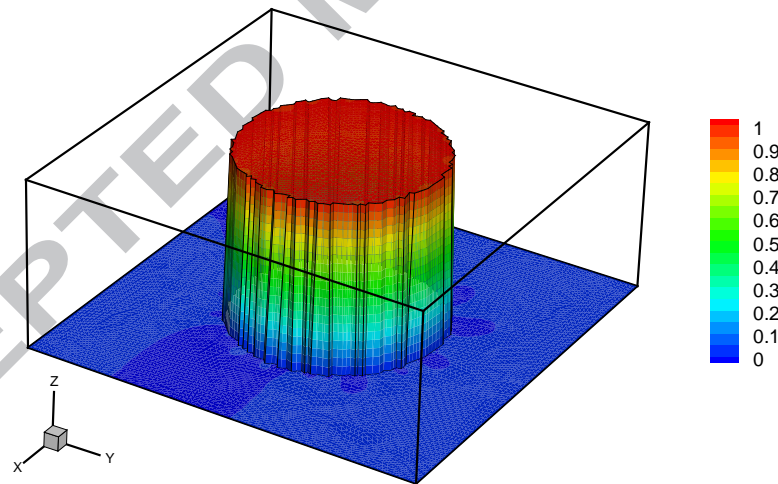


(b)

Figure 15: Spurious velocities for the mini-element with direct forcing, obtained with $h = 0.05$: (a) Q_h^1 ; (b) Q_h^Γ .

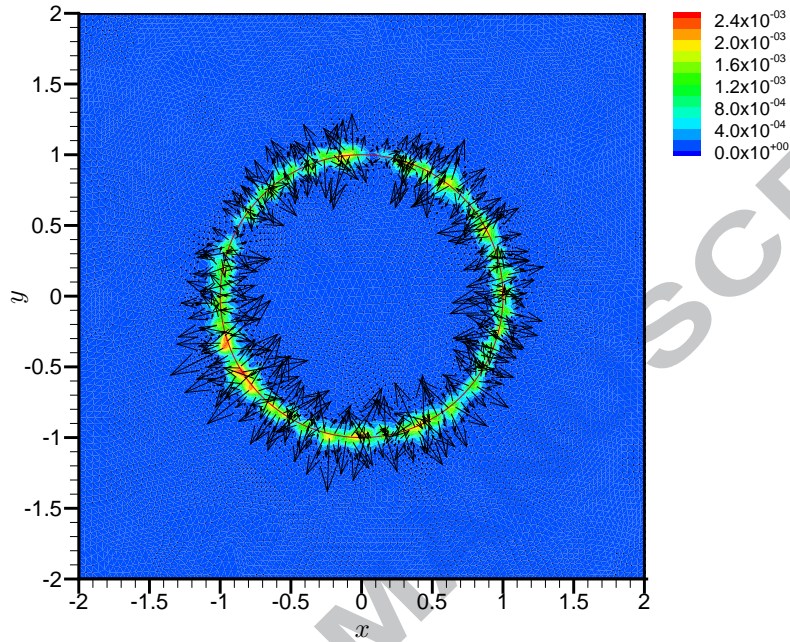


(a)

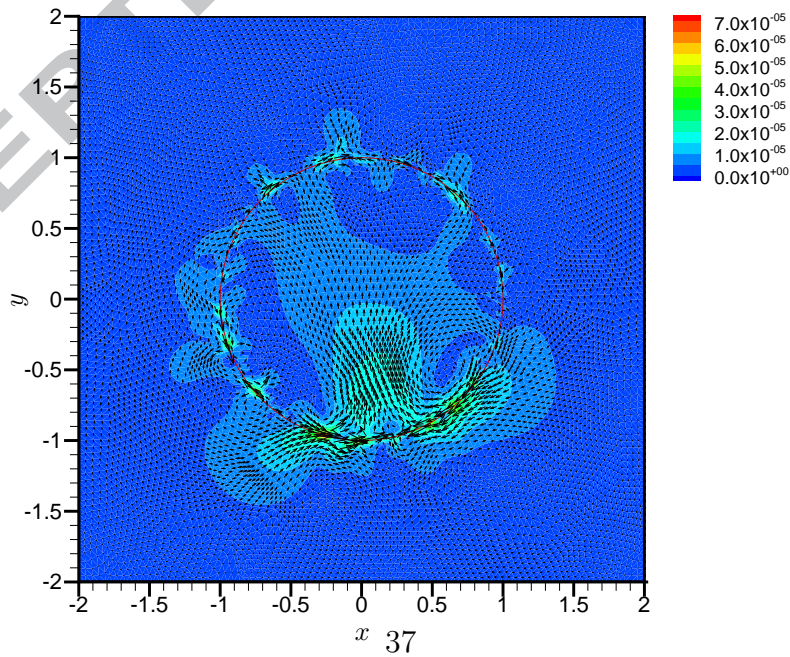


(b)

Figure 16: Pressure field for the stabilized element with Laplace-Beltrami forcing, obtained with $h = 0.05$: (a) Q_h^1 ; (b) Q_h^Γ .



(a)



(b)

Figure 17: Spurious velocities for the stabilized element with Laplace-Beltrami forcing, obtained with $h = 0.05$: (a) Q_h^1 ; (b) Q_h^r .

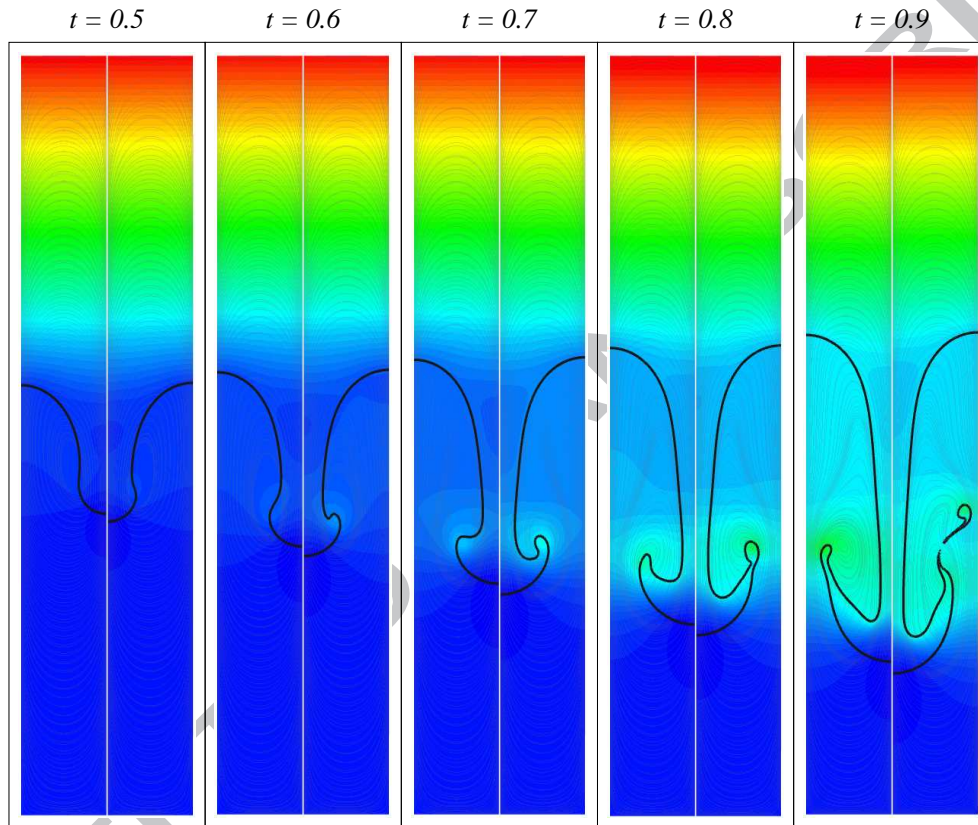


Figure 18: Two-dimensional Rayleigh-Taylor instability test case. Numerical results at times $t = 0.5, 0.6, 0.7, 0.8$ and 0.9 . The left part of each frame corresponds to $\sigma = 0.025$, while the right part corresponds to zero surface tension. Shown are color contours of the pressure (value increasing from red to blue), instantaneous streamlines, and location of the interface.

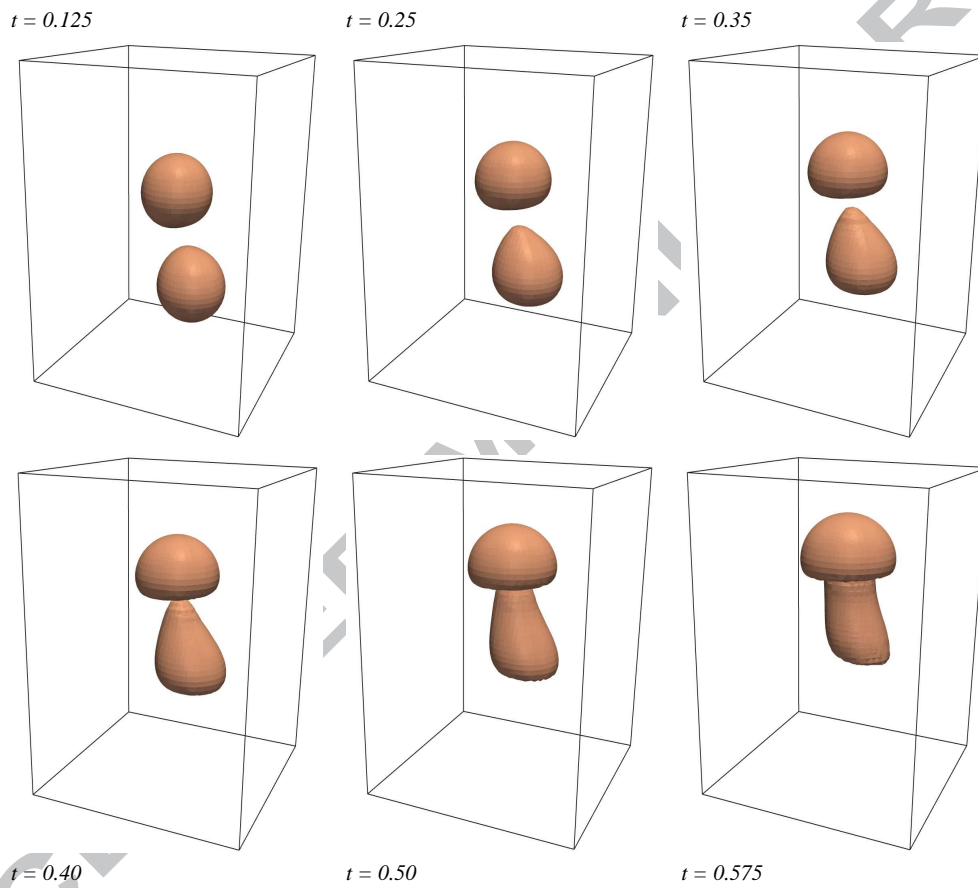


Figure 19: Merging bubbles test case. Shown are interface shapes at times $t = 0.125, 0.25, 0.35, 0.4, 0.5$ and 0.575 .

Table 1: Error $\|p - \mathcal{I}p\|_{L^2(\Omega)}$ computed for $g(x) = e^{-x}$, for the standard Q_h^1 space and for the new pressure space Q_h^Γ .

h	Q_h^1	Q_h^Γ
2.0×10^{-1}	1.332321×10^{-1}	4.166473×10^{-2}
1.0×10^{-1}	1.120209×10^{-1}	1.593032×10^{-2}
5.0×10^{-2}	7.209146×10^{-2}	4.456308×10^{-3}
2.5×10^{-2}	5.126917×10^{-2}	1.606452×10^{-3}
1.25×10^{-2}	3.607274×10^{-2}	5.286712×10^{-4}
6.25×10^{-3}	2.565891×10^{-2}	2.010631×10^{-4}
3.125×10^{-3}	1.786352×10^{-2}	6.614845×10^{-5}

Table 2: Convergence study for the Couette flow computed with the new pressure space Q_h^Γ in both stabilized (P_1/P_1) and stable (P_1^+/P_1) formulations.

h	P_1/P_1		P_1^+/P_1	
	$\ u - u_h\ _{H^1(\Omega)}$	$\ p - p_h\ _{L^2(\Omega)}$	$\ u - u_h\ _{H^1(\Omega)}$	$\ p - p_h\ _{L^2(\Omega)}$
1.76×10^{-1}	2.9635×10^{-2}	2.9413×10^{-2}	2.6850×10^{-2}	1.0408×10^{-2}
8.80×10^{-2}	1.4681×10^{-2}	8.6496×10^{-3}	1.3479×10^{-2}	3.5439×10^{-3}
4.40×10^{-2}	7.2939×10^{-3}	3.2792×10^{-3}	6.7448×10^{-3}	1.6185×10^{-3}
2.20×10^{-2}	3.6309×10^{-3}	1.1239×10^{-3}	3.3695×10^{-3}	6.6834×10^{-4}
1.10×10^{-2}	1.8115×10^{-3}	3.9940×10^{-4}	1.6833×10^{-3}	2.5230×10^{-4}